THE JOURNAL OF BIOLOGICAL CHEMISTRY VOL. 286, NO. 27, pp. 24324–24335, July 8, 2011

γ-Aminobutyric Acid Type B ($GABA_B$) Receptor Internalization Is Regulated by the R2 Subunit*[S]

Received for publication, January 14, 2011, and in revised form, April 20, 2011 Published, JBC Papers in Press, May 3, 2011, DOI 10.1074/jbc.M110.220814

Saad Hannan[‡§], Megan E. Wilkins[‡], Ebrahim Dehghani-Tafti[‡], Philip Thomas[‡], Stuart M. Baddeley[§], and Trevor G. Smart[‡1]

From the [‡]Department of Neuroscience, Physiology and Pharmacology, University College London, Gower Street, London WC1E 6BT, United Kingdom and [§]GlaxoSmithKline R&D, Medicines Research Centre, Gunnels Wood Road, Stevenage SG1 2NY, United Kingdom

γ-Aminobutyric acid type B ($GABA_B$) receptors are important for slow synaptic inhibition in the CNS. The efficacy of inhibition is directly related to the stability of cell surface receptors. For $GABA_B$ receptors, heterodimerization between R1 and R2 subunits is critical for cell surface expression and signaling, but how this determines the rate and extent of receptor internalization is unknown. Here, we insert a high affinity α-bungarotoxin binding site into the N terminus of the R2 subunit and reveal its dominant role in regulating the internalization of $GABA_B$ receptors in live cells. To simultaneously study R1a and R2 trafficking, a new α-bungarotoxin binding site-labeling technique was used, allowing α-bungarotoxin conjugated to different fluorophores to selectively label R1a and R2 subunits. This approach demonstrated that R1a and R2 are internalized as dimers. In heterologous expression systems and neurons, the rates and extents of internalization for R1aR2 heteromers and R2 homomers are similar, suggesting a regulatory role for R2 in determining cell surface receptor stability. The fast internalization rate of R1a, which has been engineered to exit the endoplasmic reticulum, was slowed to that of R2 by truncating the R1a C-terminal tail or by removing a dileucine motif in its coiled-coil domain. Slowing the rate of internalization by co-assembly with R2 represents a novel role for GPCR heterodimerization whereby R2 subunits, via their C terminus coiled-coil domain, mask a dileucine motif on R1a subunits to determine the surface stability of the $GABA_B$ receptor.

Metabotropic $GABA_B$[2] receptors mediate a slow and prolonged phase of synaptic inhibition in the CNS. Their importance for neuronal function is evident when they become dysfunctional, which can lead to a range of diseases that includes epilepsy, sleep disorders, stress, depression, and substance abuse (1–3).

Native $GABA_B$ receptors are considered to function as heterodimers formed from R1 and R2 subunits (4, 5) with the possibility that some higher order oligomeric assemblies (*e.g.* dimer of dimers) may also retain functionality (6, 7). Heterodimerization of $GABA_B$ receptors has profound consequences for their structural and functional properties, impacting on the efficiency of cell surface expression and the linkage between agonist binding and G-protein activation.

Functional $GABA_B$ receptors require both R1 and R2 to co-assemble because an endoplasmic reticulum (ER) retention motif, RSR, in the C-terminal coiled-coil domain of R1 subunits has to be masked by the R2 subunit to ensure surface expression (8, 9). Substitution of the retention motif with ASA allows R1 subunits to exit the ER and travel alone to the cell surface (8). Although the role of R2 in heterodimerization for forward trafficking has been reported, how heterodimerization, and in particular the R2 subunit, affects the cell surface stability and internalization of $GABA_B$ receptor subunits remains unresolved.

This aspect is important because the cell surface stability and mobility of $GABA_B$ receptors will directly influence the strength and duration of slow synaptic inhibition following $GABA_B$ receptor activation. Previous studies have proposed that $GABA_B$ receptors are very stable on the cell surface (10, 11), whereas more recent reports have indicated that $GABA_B$ receptors are mobile, being rapidly and constitutively internalized in the absence of agonist in both heterologous expression systems and neurons (12–15). To date, most studies addressing $GABA_B$ receptor trafficking necessarily utilized fixed cells in conjunction with surface receptor biotinylation or C-terminal antibody labeling to monitor receptor subunit mobility. However, these approaches have been unable to distinguish between the trafficking itineraries of R1 and R2, either independently or simultaneously.

By inserting the binding site motif for α-bungarotoxin (BTX) into the N terminus of the $GABA_B$ receptor R1a subunit, we have previously tracked the mobility of $GABA_B$ R1a receptors in heterologous expression systems (HEK cells) and live hippocampal neurons. Here we now insert the α-bungarotoxin binding site (BBS) into R2 subunits to monitor their independent trafficking with live cell imaging. We study how R2 affects $GABA_B$ receptor internalization and the role of heterodimerization in the trafficking of R1a and R2 subunits. By using

* This work was supported by the Medical Research Council and by a Biotechnology and Biological Sciences Research Council-GlaxoSmithKline studentship.

[S] The on-line version of this article (available at http://www.jbc.org) contains supplemental Figs. 1–6.

[1] To whom correspondence should be addressed. Tel.: 207-679-3770; Fax: 207-679-7298; E-mail: t.smart@ucl.ac.uk.

[2] The abbreviations used are: $GABA_B$, γ-aminobutyric acid type B; GABA, γ-aminobutyric acid; BTX, bungarotoxin; AF488 and AF555, Alexa Fluor 488 and 555, respectively; BBS, α-bungarotoxin binding site; BBS-CC, modified cysteine-containing BBS; CPZ, chloropromazine; DYN, dynasore; $GABA_B$ R1 and R2, γ-aminobutyric acid type B receptor subunit R1 and R2, respectively; GIRK, G-protein-activated inwardly rectifying K^+ channels; MTSES, 2-sulfonatoethyl methanethiosulfonate sodium salt; PT, near physiological temperature; VFTM, Venus flytrap module; ER, endoplasmic reticulum; DIV, days *in vitro*; eGFP, enhanced green fluorescent protein.

a new technique to differentially tag the R1a and R2 subunits with different α-bungarotoxin-linked fluorophores, we monitor the mobility of R1a and R2, simultaneously revealing a dominant role for R2 as a regulator of the rate of $GABA_B$ receptor internalization.

EXPERIMENTAL PROCEDURES

DNA Cloning and Mutagenesis—Myc-tagged $GABA_B$ R1a ($R1a^{Myc}$), BBS-tagged $GABA_B$ R1a ($R1a^{BBS}$), FLAG-tagged $GABA_B$ R2 ($R2^{FLAG}$), pEGFP-C1, and Rab7-GFP have been described previously (13, 16). eGFP-Rab5 and eGFP-Rab11 were a generous gift from José A. Esteban. The oligonucleotide sequences CTAGCTGGAGATACTACGAGAGCTCCCTGGAGCCCTACCCTGACG (sense) and CTAGCGTCAGGGTAGGGCTCCAGGGAGCTCTCGTAGTATCTCCAG (antisense), encoding the 13-amino acid BBS (WRYYESSLEPYPD) (17), were subcloned into a NheI site previously introduced into the $R2^{FLAG}$ subunit such that the BBS was placed 27 amino acids from the start of the mature protein (Fig. 1*A*). The $GABA_BR2^{BBS}$ ($R2^{BBS}$) cDNA was subcloned into a pRK5 vector. The ER retention motif of $GABA_B$ $R1a^{BBS}$ was mutated from RSR to ASA ($R1a^{BBS\text{-}ASA}$) using an inverse PCR method and oligonucleotides GCCTCAGCGCGCCACCCCCCAACACCCCCAGATC (forward primer) and GAGTTGCTGCCGAGACTGGAGCTG (reverse primer). $R1a^{BBS}$ with a complete truncation of the C-terminal tail (starting after Arg^{858}), $R1a^{BBS}\Delta CT$, was made from $R1a^{BBS}$ using an inverse PCR method and the oligonucleotides TAGTTTAGAGTCGGCCTGCAGAA (forward primer) and CCTGCGCATCTTGGGCACAAAGAG (reverse primer). Two leucines were substituted with alanines (L889A,L890A) in $R1^{BBS\text{-}ASA}$ by an inverse PCR with the primers GCAGCAGAGAAGGAAAACCGAGAACTG (forward) and TCGGGACTTCTCTTCCTCGTTGTT (reverse). R2 with a truncated C-terminal tail (truncation starting after Thr^{748}; R2ΔCT) was made from $R2^{FLAG}$ using an inverse PCR method and the oligonucleotides TAGAAGCTTGGCCGCCATGGCCCAA (forward primer) and GTTTGTCCTCAGAGTGATGAGCTTTG (reverse primer). Two serine residues in the BBS were substituted with cysteines in $R1a^{BBS}$ by an inverse PCR method using TGTTGTCTGGAGCCCTACCCTGACGCTAGC (forward primer) and CTCGTAGTATCTCCAGCTAGCTA (reverse primer) to create an R1 with modified BBS for double fluorophore labeling ($R1a^{BBS\text{-}CC}$). The entire cDNA sequences of all constructs were checked for fidelity.

Cell Culture and Transfection—HEK-293 cells stably expressing potassium channels, Kir3.1 and Kir3.2 (GIRK cells), were maintained at 37 °C and 95% air, 5% CO_2 in DMEM supplemented with 10% fetal calf serum (FCS), penicillin-G/streptomycin (100 units/100 μg/ml), 2 mM glutamine, and Geneticin (0.5 mg/ml) (all from Invitrogen). Cells were seeded onto poly-L-lysine-coated 22-mm glass coverslips and transfected using a calcium phosphate method (13) with 4 μg of total DNA in the following ratios: R1a (or $R1a^{BBS}$)/R2 (or $R2^{BBS}$)/eGFP reporter (1:5:1) or R1a (or $R1a^{BBS}$)/R2 (or $R2^{BBS}$) (1:5). For radioligand binding experiments, cells were transfected by electroporation using a GenePulser II electroporator (Bio-Rad) (18) using 10 μg of DNA with an R1a/$R2^{BBS}$ ratio of 1:3 and then plated onto 10-cm dishes at 70% confluence.

Dissociated E18 rat hippocampal neurons were cultured on poly-D-lysine-coated 18- or 22-mm glass coverslips (Assistance/VWR) in a medium containing MEM, 5% (v/v) heat-inactivated FCS, 5% (v/v) heat-inactivated horse serum, penicillin-G/streptomycin (10 units/10 μg/ml), 2 mM glutamine (Invitrogen), and 20 mM glucose (Sigma). After 3 h, the plating medium was replaced with Neurobasal-A supplemented with 1% (v/v) B-27, penicillin-G/streptomycin (50 units/50 μg/ml), 0.5% (v/v) Glutamax (Invitrogen), and 35 mM glucose. The neurons were maintained in this medium before transfection at 8–10 DIV using Effectene (Qiagen) or calcium phosphate (19).

α-Bungarotoxin Radioligand Binding Assay—The apparent affinity of BTX for its binding site on the $GABA_B$ $R1aR2^{BBS}$ receptor was determined using ^{125}I-BTX as described previously (13). GIRK cells expressing $R1aR2^{BBS}$ were washed in PBS before resuspension in PBS containing 0.5% (w/v) bovine serum albumin (BSA; Sigma). Cells were incubated in 150 μl of PBS plus BSA containing ^{125}I-BTX (200 Ci/mmol; PerkinElmer Life Sciences) for 60 min at room temperature. Nonspecific binding was determined after the addition of a 1000-fold excess higher concentration of unlabeled BTX (Molecular Probes). Radioligand binding was assessed by filtration onto 0.5% polyethyleneimine presoaked Whatman GF/A filters, followed by rapid washing with PBS using a Brandel cell harvester. The radiolabel retained on the filters was assayed with a Wallac 1261 γ counter. Scatchard analysis with non-linear regression was used to obtain B_{max} and K_d values from the equation,

$$y = (B_{max}X)/(K_d + X) \quad \text{(Eq. 1)}$$

where X represents the ^{125}I-BTX concentration. The same analysis was used for the $\alpha7/5HT_{3a}$ receptor chimera, expressed in GIRK cells, which exhibits high affinity BTX binding (13).

Whole-cell Electrophysiology—Whole-cell potassium currents activated by GABA were recorded from individual $GABA_B$ receptor-expressing GIRK cells using patch clamp recording as indicated previously (13). Patch pipettes (resistances: 3–5 megaohms) contained the following solution: 120 mM KCl, 2 mM $MgCl_2$, 11 mM EGTA, 30 mM KOH, 10 mM HEPES, 1 mM $CaCl_2$, 1 mM GTP, 2 mM ATP, 14 mM creatine phosphate, pH 7.0. The GIRK cells were bathed in a Krebs solution containing 140 mM NaCl, 4.7 mM KCl, 1.2 mM $MgCl_2$, 2.5 mM $CaCl_2$, 11 mM glucose, and 5 mM HEPES, pH 7.4. To increase the amplitude of the $GABA_B$ receptor-activated K^+ currents, prior to the application of GABA, the KCl concentration in the external solution was increased to 25 mM, with a corresponding reduction in the NaCl concentration to 120 mM. This shifted E_K from −90 to −47 mV. The peak amplitude GABA-activated K^+ currents were now inward at a holding potential of −70 mV. Membrane currents were recorded from cells 48–72 h post-transfection and filtered at 5 kHz (−3 dB, 6th pole Bessel, 36 dB/octave) before storage on a Dell Pentium III computer for analysis with Clampex 8. Changes >10% in the membrane input conductance or series resistance resulted in the recording being discarded.

The GABA concentration response curves were generated by measuring the potassium current (I) for each GABA concentration applied at 3-min intervals in the absence or presence of 3 μg/ml BTX coupled to AlexaFluor 555 (BTX-AF555; Molecular Probes). The current amplitudes were normalized to the maximum GABA response (I_{max}), and the concentration response relationship was fitted with the Hill equation,

$$I/I_{max} = ((1/1 + (EC_{50}/A)^n)) \quad \text{(Eq. 2)}$$

where A represents GABA concentration, EC_{50} is the concentration activating 50% of the maximum response, and n is the Hill slope.

Double Labeling of R1a and R2 with BTX—R1a and R2 subunits containing the Cys mutant ($R1a^{BBS\text{-}CC}$) and wild-type ($R2^{BBS}$) versions of the BBS were exposed to 0.2 mM dithiothreitol (DTT) in PBS for 15 min at room temperature. After washing (three times) in PBS, cells were incubated with 200 μM MTSES in PBS for 5 min at 4 °C to selectively block the binding of BTX to $R1a^{BBS\text{-}CC}$. Subsequently, after washing in ice-cold PBS (three times), the cells were incubated in 3 μg/ml BTX coupled to Alexa Fluor 488 (BTX-AF488; Molecular Probes) for 10 min at 4 °C to label the $R2^{BBS}$ subunits. The cells were then washed with PBS (three times) to remove the unbound BTX-AF488 and incubated in 2 mM DTT in ice-cold PBS for 5 min at room temperature to remove the MTSES bound to $R1a^{BBS\text{-}CC}$ subunits. The cells were then washed with PBS to remove the DTT and finally incubated in 3 μg/ml BTX-AF555 for 10 min at 4 °C to label the $R1a^{BBS\text{-}CC}$ subunits. Finally, PBS was used to remove excess BTX-AF555 prior to dual fluorophore confocal imaging.

Fixed Cell Imaging—Cells were fixed in 4% (w/v) paraformaldehyde in PBS for 5 min and quenched with 5% (w/v) NH_4Cl in PBS for 5 min. After washing (three times), cells were mounted on glass slides using glycerol. A Zeiss Axioskop LSM510 confocal microscope with three laser lines (λ = 488, 543, and 643 nm) and a Meta head was used with a Plan Neofluor 40× oil differential interference contrast objective (numerical aperture 1.3) for imaging. The top and bottom of the imaged cell was determined using a rapid z-stack scan, and a mid-stack slice was optimized and acquired as a mean of four scans in 8 bits and stored for analysis.

Live Cell Imaging—Live transfected GIRK cells and hippocampal neurons (12–14 or 19–21 DIV) were imaged using the confocal microscope with an Achroplan 40× water immersion differential interference contrast objective (numerical aperture 0.8). To label $R1a^{BBS}$ or $R2^{BBS}$ with BTX, transfected GIRK cells were washed three times in Krebs and incubated in 3 μg/ml BTX-AF555. Transfected hippocampal neurons were similarly washed and incubated in 1 mM D-tubocurarine for 5 min to prevent BTX binding to native nicotinic acetylcholine receptors, followed by incubation with 3 μg/ml BTX-AF555 in Krebs for 10 min. Labeled cells were superfused with Krebs at 16–18, 22–24, or 30–32 °C.

To start imaging at $t = 0$, the top and bottom of the cell were determined with a rapid z-scan. The mid-optical slice was optimized and imaged as a mean of four scans in 8 bits using the 543-nm helium-neon laser (560-nm long pass filter) for BTX-AF555 or the 488-nm argon laser (505–530-nm band pass filter) for imaging eGFP or BTX-AF488. For later time points, all of the confocal settings (detector gain, amplifier offset, optical slice thickness, and laser intensity) were unaltered from those used at $t = 0$. For fixed and live cell imaging at low temperatures, cells were co-transfected with eGFP and $GABA_B$ receptor subunit constructs. For single fluorophore live cell confocal imaging at room and near physiological temperatures, the cells were only transfected with the receptor subunits. Thus, the only fluorophore excited during live cell imaging was AF555, conjugated to α-BTX. This minimized the exposure time of the cells to the laser. During live imaging, transmitted light or eGFP images were captured simultaneously with BTX-AF555 images to check for change to cell morphology. The majority of cells showed no sign of phototoxicity, such as surface blebbing, over 1-h periods of imaging, and those that did were excluded from analysis.

Photobleaching Profile—To ensure that the rate and extent of $R1a^{BBS}R2$ receptor internalization could be accurately measured using the BTX-linked fluorophores required that the fluorophores not be significantly affected by photobleaching. To determine the extent of any photobleaching for BTX-AF555, live GIRK cells, transfected with $R1a^{BBS}R2$, were tagged with BTX-AF555 and then exposed to eight scans (pixel time = 1.6 μs) performed consecutively every 8 s up to a total of 120 (total laser exposure time per pixel = 192 μs) at 7–9 °C and 30–32 °C. A loss of ~10% fluorescence intensity was evident over 120 scans, which was unaffected by temperature. However, this rate of scanning far exceeds that used in all of the live cell experiments, which required four scans at 5 time points over 1 h, giving a total of just 20 scans. Therefore, photobleaching was negligible and did not affect the surface fluorescence measurements.

Image Analysis—Confocal images were analyzed using ImageJ (version 1.40g) (National Institutes of Health, Bethesda, MD). The mean fluorescence was determined for three regions of interest, selected for each cell: surface membrane, intracellular compartment, and total cell fluorescence. Background fluorescence was set by imaging a region of the coverslip devoid of cells. This was subtracted from the region of interest fluorescence, yielding a mean background-corrected fluorescence. For live cells, the mean background-corrected fluorescence per unit area (μm^2) at each time point was then normalized to the mean background-corrected fluorescence/μm^2 at $t = 0$. These values were then fitted with an monoexponential decay function using Origin (version 6).

RESULTS

Constitutive Internalization of $GABA_BR1a^{BBS}R2$ Heterodimers in Live Cells—To determine how the α-BTX tagging method performed in live rather than fixed cells, we studied the temperature dependence of the rate and extent of constitutive internalization of $R1a^{BBS}R2$ receptors expressed in GIRK cells and cultured hippocampal neurons. The loss of surface fluorescence over time (1 h) was used as a rate indicator of BTX-labeled $GABA_B$ $R1a^{BBS}R2$ internalization, sampled at low (16–18 °C), room (22–24 °C), or near physiological (30–32 °C; PT) temperatures. The extent of internalization is the percentage of receptors at $t = 0$ remaining at

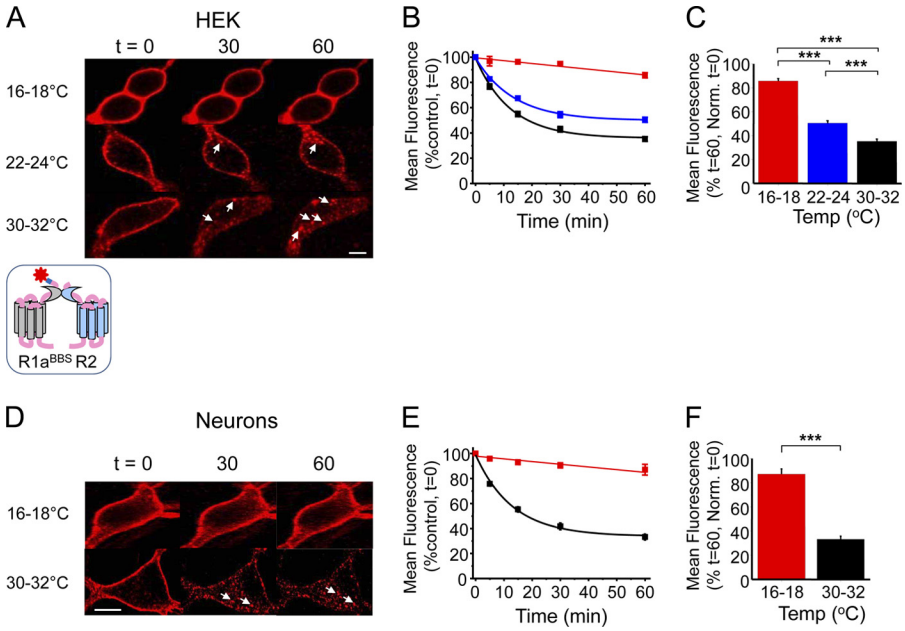

FIGURE 1. **Constitutive internalization of R1a^{BBS}R2 receptors in live GIRK cells and neurons.** *A*, GIRK cells expressing R1a^{BBS}R2 receptors were incubated in 3 μg/ml BTX-AF555 for 10 min at room temperature and then imaged over 0–60 min at 16–18, 22–24, and 30–32 °C. The *arrowheads* indicate internalized R1a subunits. *Scale bar*, 5 μm. *B and C*, rate (*B*) and extent (*C*) of internalization of BTX-AF555-tagged R1a^{BBS}R2 at 16–18 °C (*red*), 22–24 °C (*blue*), and 30–32 °C (*black*). $n = 6–15$; ***, $p < 0.001$. In this and following figures, all *points* and *bars* represent means ± S.E. (*error bars*). *D*, Hippocampal neurons (14–21 DIV) expressing R1a^{BBS}R2 and eGFP were incubated in 1 mM d-tubocurarine for 5 min followed by 3 μg/ml BTX-AF555 for 10 min at room temperature and imaged at different time points at 16–18 °C or 30–32 °C. The *arrowheads* indicate internalized R1a subunits. *Scale bar*, 10 μm. *E and F*, rate (*E*) and extent (*F*) of internalization of BTX-AF555-tagged R1a^{BBS}R2 receptors at 16–18 °C (*red*) and 30–32 °C (*black*) in live hippocampal neurons, $n = 6–12$. ***, $p < 0.001$.

TABLE 1

Rates and extents of GABA$_B$ receptor internalization

Cells	Construct	Temperature	Rate (n)[a]	Extent (n)
		℃	*min*	%
GIRK cells	R1a^{BBS}R2	16–18		86 ± 2 (6)
		22–24	13.4 ± 1.4 (7)	51 ± 2
		30–32	12.4 ± 1.1 (15)	35 ± 2
	R1a^{BBS}R2 + DYN	30–32	13.7 ± 2.6 (11)	49.3 ± 3.6
	R1a^{BBS}R2 + CPZ	30–32	10.4 ± 1.8 (5)	52.4 ± 4.1
	R1a$^{BBS\text{-}ASA}$	22–24	7.2 ± 1.5 (10)	30 ± 3
	R1a$^{BBS}\Delta$CT	22–24	15.0 ± 1.4 (6)	41 ± 2
	R1a$^{BBS\text{-}LL889–90AA}$	22–24	11.4 ± 2.6 (6)	47 ± 4
	R1a$^{BBS\text{-}LL889–90AA}$ R2ΔCT	22–24	9.0 ± 2.0 (6)	32 ± 2
	R2^{BBS}	16–18		85 ± 2 (5)
		22–24	18 ± 3 (8)	47 ± 2
		30–32	12.4 ± 1.1(10)	31 ± 1
	R1aR2^{BBS}	16–18		90 ± 2 (7)
		22–24	18.8 ± 2.2 (13)	48 ± 2
		30–32	16.4 ± 2.2 (6)	30 ± 1
Neurons	R1a^{BBS}R2	16–18		87 ± 4 (6)
		30–32	13.1 ± 1.7 (12)	33 ± 3
	R1aR2^{BBS}	16–18		89 ± 2 (7)
		30–32	17.1 ± 3.2 (14)	33 ± 2
Neurons, double labeling	R1a$^{BBS\text{-}CC}$	30–32	11 ± 1 (5)	32 ± 3
	R2^{BBS}	30–32	8 ± 1 (5)	35 ± 3

[a] n = number of experiments.

$t = 60$, which reflects a steady state that is attained between internalization and the recycling of receptors.

GIRK cells expressing R1a^{BBS}R2 and eGFP and exposed to 3 μg/ml BTX-AF555 for 10 min at room temperature exhibited clear surface labeling of R1a^{BBS} subunits (supplemental Fig. 1*A*). Similar labeling was apparent with cultured hippocampal neurons expressing R1a^{BBS}R2 and eGFP following preincubation with 1 mM D-tubocurarine for 5 min (supplemental Fig. 1*B*). Such labeling was not observed when transfected cells were incubated either with unconjugated BTX or if cells expressed only eGFP and were incubated with BTX-AF555 (supplemental Fig. 1, *A* and *B*).

Low temperatures (16–18 °C), which impede internalization (20), stabilized the surface fluorescence for up to 1 h with minimal loss (<13%; Fig. 1, *A–D*, and Table 1), indicating that at these low temperatures, GABA$_B$ receptors undergo very little constitutive internalization. This result, together with our photobleaching profiles (supplemental Fig. 2, *A* and *B*), demonstrated that over 1 h, fluorophore photobleaching was insignificant.

By contrast, at room temperature and PT, R1a^{BBS}R2 rapidly and constitutively internalized in GIRK cells (Fig. 1*B* and Table 1). Within 5 min at PT, intracellular compartments were decorated with internalized BBS-tagged receptors (Fig. 1*A*).

Although the rates of internalization at room temperature and PT appeared similar (Fig. 1*B*), the extent of internalization after 1 h was significantly greater at higher temperature compared with room temperature, and these were both significantly greater than the extent of internalization at 16–18 °C (Fig. 1*C* and Table 1).

Similar constitutive internalization of R1a^{BBS}R2 was evident in transfected hippocampal neurons (14–21 DIV) at PT. Intracellular structures again filled with BTX-AF555-tagged receptors within 5 min (Fig. 1, *D* and *E*), and after 1 h, the extent of receptor internalization was considerably greater than at 16–18 °C (Fig. 1*F* and Table 1).

Labeling GABA$_B$ receptors with BTX linked to fluorophores did not cause any changes in the morphology of the transfected cells (supplemental Fig. 3, *A* and *B*).

Real-time Internalization of GABA$_B$ Receptors by Clathrin- and Dynamin-dependent Mechanisms—To monitor internalization in real time over 1 h, live GIRK cells expressing R1a^{BBS}R2 receptors were labeled with BTX-AF555 at 30–32 °C. Compared with untreated controls ($\tau = 12.4 \pm 1.1$ min; $n = 15$), the rate of internalization for R1a^{BBS}R2 was unaffected by either the inhibitor of clathrin-coated pit formation, chlorpromazine (14) (50 μg/ml CPZ; $\tau_{CPZ} = 10.4 \pm 1.8$ min, $n = 5$), or the cell-permeable inhibitor of dynamin GTPase activity, dynasore (21) (80 μM DYN; $\tau_{DYN} = 13.7 \pm 2.6$ min, $n = 11$, $p > 0.05$; Fig. 2*A*). However, both chlorpromazine (52.4 ± 4.1%, $n = 5$, $p < 0.01$) and dynasore (49.3 ± 3.6, $n = 11$, $p < 0.01$) significantly reduced the extent of internalization compared with controls (Fig. 2*B*).

The fate of the internalized R1a^{BBS}R2 receptors was assessed by co-staining for intracellular structures. Hippocampal neurons were co-transfected with markers for early endosomes (eGFP-Rab5) (22, 23), for recycling endosomes (eGFP-Rab11) (24, 25), and for late endosomes/lysosomes (Rab7-GFP) (26). Surface receptors were labeled with BTX-AF555 for 10 min at room temperature and washed in Krebs prior to incubation at 37 °C for 30–60 min to allow the BTX-tagged receptors to internalize. The BTX-AF555 tagged R1a^{BBS}R2 co-localized with GFP-tagged Rab5, Rab11, and Rab7 containing intracellular compartments in the soma and dendrites of cultured hippocampal neurons (Fig. 2*C*). Therefore, after being internalized, GABA$_B$ receptors are recruited to early endosomes, from where they are either recycled via recycling endosomes to be reinserted into the plasma membrane or are degraded in the lysosomes via the late endosomes, consistent with previous findings (14, 15, 27, 28). The process of recycling would account for the plateau phase in the time profiles of surface fluorescence (Fig. 2).

R1a Homomers Internalize Faster and More Extensively than R1aR2 Heterodimers—To determine the importance of heterodimerization on constitutive internalization of GABA$_B$ receptors, the trafficking of R1a and R2 were studied individually. For R1a to internalize in the absence of R2, its ER retention motif (-RSR) was substituted for -ASA (R1a$^{BBS\text{-}ASA}$).

In GIRK cells expressing only BTX-AF555-labeled R1a$^{BBS\text{-}ASA}$ on the cell surface at room temperature, there was clear evidence of constitutive internalization (Fig. 3*A*). Intracellular structures were decorated even at $t = 0$, indicating active receptor internalization during BTX-AF555 binding. The loss of surface fluorescence for R1a$^{BBS\text{-}ASA}$ was significantly faster (Fig. 3, *B* and *C*, and Table 1) and more extensive after 60 min (Fig. 3*D* and Table 1) compared with R1a^{BBS}R2 heterodimers.

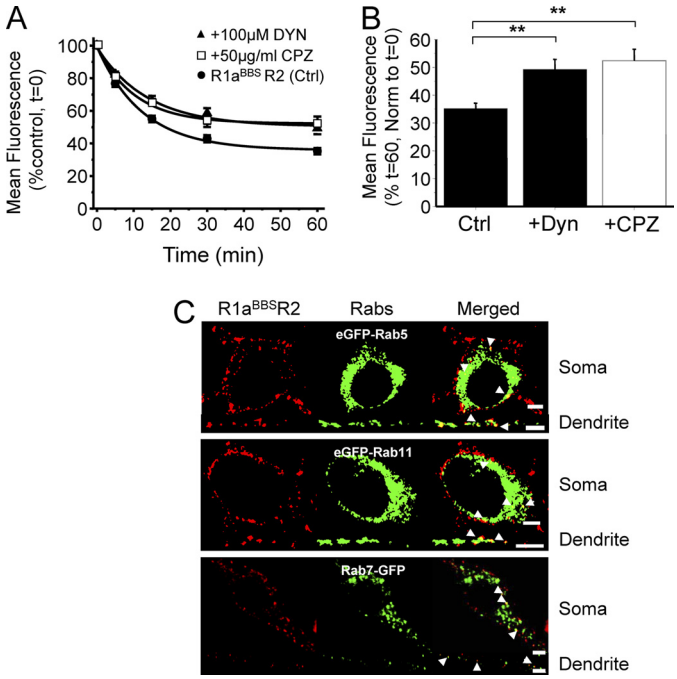

FIGURE 2. **GABA$_B$ receptors are internalized via clathrin and dynamin-dependent mechanisms and recruited to lysosomes.** Shown are the rate (*A*) and extent (*B*) of constitutive internalization of BTX-AF555-tagged R1a^{BBS}R2 receptors in the absence (●) and presence of dynasore (▲) or chlorpromazine (□). GIRK cells expressing R1a^{BBS}R2 receptors were incubated in 3 μg/ml BTX-AF555 for 10 min at room temperature and imaged over 0–60 min at 30–32 °C in the presence of either 50 μg/ml CPZ or 80 μM DYN, $n = 5$–11. **, $p < 0.05$ (one-way ANOVA). *C*, hippocampal neurons (14–21 DIV) expressing R1a^{BBS}R2 and either eGFP-Rab5, eGFP-Rab11, or Rab7-eGFP were incubated in 1 mM D-tubocurarine for 5 min, followed by 3 μg/ml BTX-AF555 for 10 min at room temperature. Cells were incubated at 37 °C for 30–60 min and then fixed and imaged. The *arrowheads* depict co-localization in the soma (*top*) and a dendrite (*bottom*). *Scale bars*, 5 μm; *error bars*, S.E.

The slower rate of internalization for R1a^{BBS}R2 could be due to a dominant internalization signal on R1a being masked by heterodimerization with R2. R2 subunits interact closely with R1a in the C-terminal coiled-coil domain and the N-terminal Venus flytrap module (VFTM).

To determine if the R1a C-terminal tail contains a dominant internalization signal, a tailless R1a^{BBS} receptor was generated in which the C terminus was truncated from and including Leu^{859} (R1a$^{BBS}\Delta$CT). This subunit was expressed on the GIRK cell surface without R2 because the truncation included the ER retention motif. Constitutive internalization of BTX-labeled R1a$^{BBS}\Delta$CT (Fig. 3*A*) proceeded at a rate and to an extent very similar to that for R1a^{BBS}R2 (Fig. 3, *B*, *C*, and *D*, and Table 1).

These data suggest that R2 subunits are a major determinant of the rate of trafficking for R1a when co-assembled as a heterodimer and that the R1a C-terminal tail contains an endocytic signal that, in the absence of R2, causes R1a subunits to constitutively internalize at a faster rate and to a greater extent than the dimer.

Inserting a Bungarotoxin Binding Site on GABA$_B$ R2—To directly establish that R2 subunits are determining the rate of

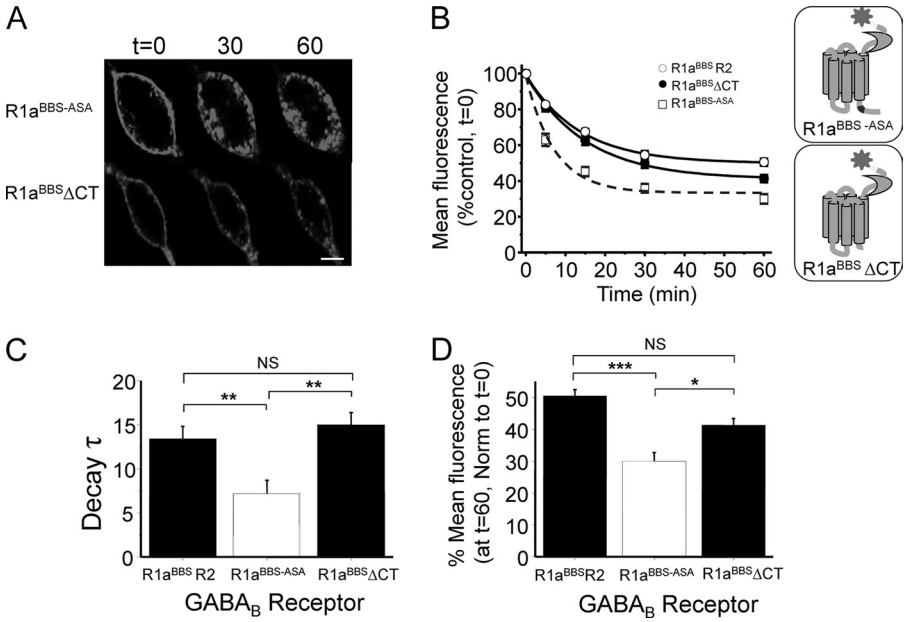

FIGURE 3. **Faster and more extensive internalization of R1a$^{BBS-ASA}$ compared with R1a^{BBS}R2.** *A*, GIRK cells expressing either R1a$^{BBS-ASA}$ (*top*) or R1a^{BBS}ΔCT (*bottom*) were incubated in 3 μg/ml BTX-AF555 for 10 min at room temperature to label surface GABA$_B$ receptors and imaged over 0–60 min at room temperature. *B*, the rate of internalization of BTX-AF555-tagged R1a^{BBS}R2 heteromers and R1a$^{BBS-ASA}$ and R1a^{BBS}ΔCT homomers at room temperature (n = 6–10). The *inset* shows the relative positions of the ASA motif and C-terminal truncation (ΔCT). *C*, exponential decay time constants (min) for surface R1a^{BBS}R2, R1a$^{BBS-ASA}$, and R1a^{BBS}ΔCT. *D*, extent of internalization for R1a^{BBS}R2, R1a$^{BBS-ASA}$, or R1a^{BBS}ΔCT. One-way analysis of variance was used. *, $p < 0.05$; **, $p < 0.01$; ***, $p < 0.001$. *Scale bar*, 5 μm; *NS*, not significant; *error bars*, S.E.

internalization of R1aR2 heterodimers required a separate BBS to be inserted into the R2 subunit. This was placed in the N terminus 27 residues from the start of the mature R2 protein (Fig. 4*A*). Clear and specific labeling with BTX-AF555 (3 μg/ml) was observed in GIRK cells and neurons co-expressing R1aR2^{BBS} and eGFP (Fig. 4, *B* and *C*). No labeling was observed with unconjugated BTX or in cells expressing only eGFP (supplemental Fig. 4).

The functional neutrality of the BBS in R2 was assessed using whole-cell patch clamp recording. GIRK cells stably expressing inwardly rectifying potassium channels (Kir3.1 and Kir3.2) were used to express either R1aR2^{BBS} or R1aR2. GABA concentration response curves for activating Kir3.1 and 3.2 were overlapping for R1aR2 and R1aR2^{BBS}, reflecting similar GABA potencies with EC$_{50}$ values of 0.5 ± 0.1 μM (R1aR2^{BBS}; n = 6–7) and 0.4 ± 0.04 μM (R1aR2; n = 7–13, $p > 0.05$; Fig. 4*D*).

Occupation of the BBS by preincubation for 10 min with unlabeled BTX did not affect the GABA curves or their EC$_{50}$ values (R1a^{BBS}R2, 0.53 ± 0.01 μM, n = 5; R1aR2^{BBS}, 0.8 ± 0.1 μM, n = 5), compared with those for wild-type R1aR2. Thus, inserting the BBS into R2 had no significant effect on the functional properties of R1a R2^{BBS}.

To determine the apparent affinity of BTX for the BBS on R2, radioligand binding with ^{125}I-BTX was used. The binding curve for ^{125}I-BTX to R1aR2^{BBS} expressed in GIRK cells saturated at ~100 nM (Fig. 4*E*). Scatchard analysis revealed a K_d for BTX binding of 45.5 ± 4.8 nM (n = 6). This was 4-fold lower than the K_d for BTX binding to the R1a^{BBS}R2 receptor (9.8 ± 2.6 nM; n = 6) (13). As a control, ^{125}I-BTX binding to the nicotinic α7/5HT$_{3A}$ chimera was determined. This revealed an innate high affinity BTX binding site (29) with a K_d of 3.92 ± 2.4 nM (n = 3), close to that previously reported.

R2 Homomers Internalize at the Same Rate as R1aR2 Heterodimers—Because R2 subunits can form homomeric surface receptors (6), GIRK cells expressing R2^{BBS} were used to determine the rate and extent of constitutive R2 internalization and to establish its regulatory role in heterodimer internalization.

R2 subunits, labeled with BTX-AF555 at room temperature, showed clear surface expression. At 16–18 °C, internalization of R2^{BBS} was minimal but rapidly increased in rate and extent at room temperature and PT (Fig. 5*A* and supplemental Fig. 5*A*) with rates and extents of constitutive internalization that were comparable with those for R1a^{BBS}R2 ($p > 0.05$; Table 1). By contrast, the rate of internalization for R2^{BBS} was slower, and its extent was reduced (Fig. 5*B* and Table 1) compared with that for R1a^{ASA} at room temperature.

To ensure that there was no contamination from unexpected innate expression of R1a in GIRK cells, GABA was applied during whole-cell patch clamp recording of cells expressing R2^{BBS} and identified by BTX-AF555. Even with 1 mM GABA, no potassium currents were activated (n = 6; data not shown), indicating the absence of endogenous R1 subunits. Therefore, the rate and extent of internalization genuinely reflect those of R2^{BBS}.

To determine the influence of R2^{BBS} on the internalization of the heterodimer, R1aR2^{BBS} was expressed in GIRK cells (Fig. 5*A* and supplemental Fig. 5*B*). The rate and extent of internalization were comparable with those for either R1a^{BBS}R2 heteromers or R2^{BBS} homomers with low temperatures minimizing internalization of R1aR2^{BBS} (Fig. 5*A*), which rapidly increased at room temperature and PT (Fig. 5*A* and Table 1). However, the rate of internalization for R1aR2^{BBS} was slower, and the extent was reduced compared with R1a$^{BBS-ASA}$ (Fig. 5*B*). These

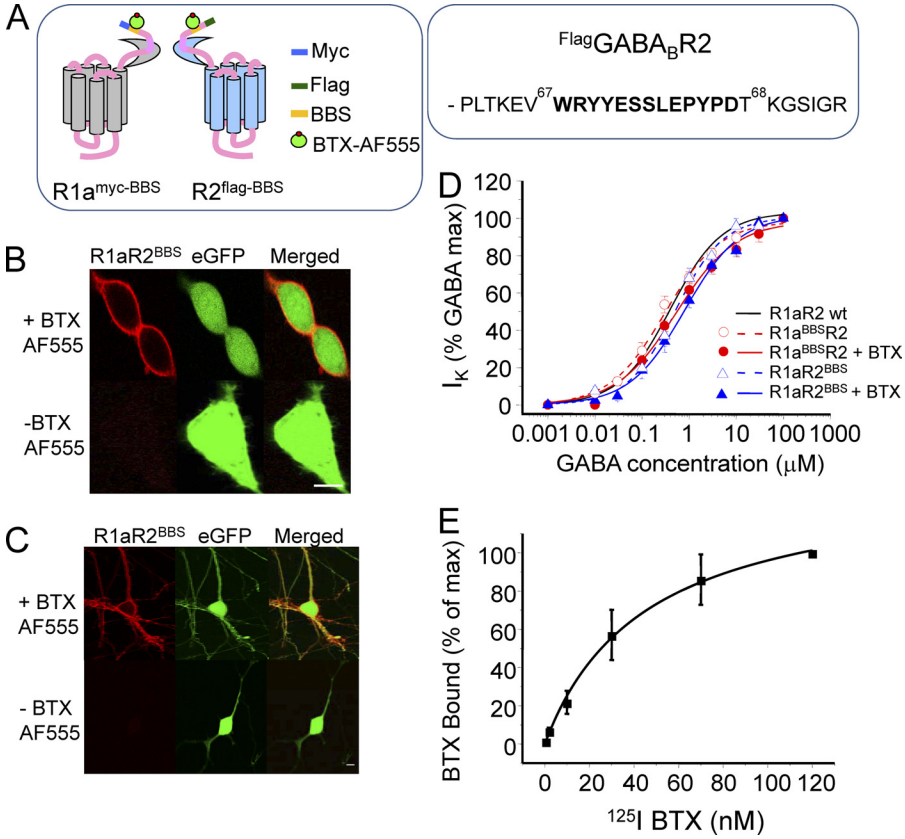

FIGURE 4. **Silent incorporation of the BBS into R2 subunits.** *A*, schematic diagram showing the relative locations for the BBS and the Myc and FLAG epitopes in GABA$_B$ R1a and R2 subunits. For the R2 subunit, the BBS was inserted between Val^{67} and Thr^{68}, as shown in the segment of the primary sequence. *B*, images of GIRK cells expressing R1aR2^{BBS} and eGFP were incubated with (+) or without (−) 3 μg/ml BTX-AF555 for 10 min at room temperature. *C*, images of rat cultured hippocampal neurons expressing R1aR2^{BBS} and eGFP, incubated with 1 mM D-tubocurarine for 5 min followed by incubation with or without 3 μg/ml BTX-AF555 for 10 min at room temperature. *Scale bars*, 5 μm. *D*, GABA concentration response curves for R1aR2, R1aR2^{BBS}, and R1a^{BBS}R2 receptors and BTX-bound R1aR2^{BBS} and R1a^{BBS}R2 receptors all expressed in GIRK cells (n = 5–13). *E*, whole-cell radioligand binding experiments with ^{125}I-BTX for the R1aR2^{BBS} receptor (n = 6). *Error bars*, S.E.

data suggest that R2 subunits play a dominant role in determining the rate and extent of constitutive internalization of R1a subunits when co-assembled in a heterodimer.

Constitutive internalization of R1aR2^{BBS} receptors was also evident in the soma of 14–21-DIV cultured hippocampal neurons. As expected, internalization of R1aR2^{BBS} rapidly increased from 16–18 to 30–32 °C (Fig. 5*C*, supplemental Fig. 5*C*, and Table 1), being very similar in profile to R1a^{BBS}R2. This indicated that the receptors are probably internalized as heterodimers.

Dileucine Motif on R1a Is a Dominant Positive Signal for Internalization—R2 subunits may regulate the stability of cell surface GABA$_B$ receptors by interacting with a dominant endocytic sorting signal on the R1a C-tail. Given that a dileucine motif in the R1a coiled-coil domain (Leu^{889}, Leu^{890}) can affect the surface availability of GABA$_B$ receptors (8, 30), the consequences of their replacement by alanines were investigated on the background of R1a$^{BBS-ASA}$ forming R1a$^{BBS-ASA,L889A,L890A}$.

The rate and extent of internalization for BTX-labeled R1a$^{BBS-ASA,L889A,L890A}$ in GIRK cells at room temperature (Fig. 6, *A* and *B*) were similar to that for R1a^{BBS}R2, R1aR2^{BBS}, and R2^{BBS} (Fig. 6, *C* and *D*, and Table 1). However, the extent of internalization for R1a$^{BBS-ASA,L889A,L890A}$ was significantly less when compared with R1a$^{BBS-ASA}$ (Fig. 6*D*). This is in accord with the dileucine motif acting as a dominant endocytic signal, and upon heterodimerization with R2, this motif is inactivated via an interaction of the coiled-coil domains, thereby increasing the stability of the R1aR2 heterodimer on the cell surface.

To examine this putative role for the R2 C-tail in determining the rate of internalization of R1a subunits, the C-tail was truncated (R2ΔCT) starting from and including Asn^{749}. The R1a$^{BBS-ASA}$R2ΔCT receptors will still interact via their N-terminal VFTMs, but the dileucine motif on R1a will now be freed from the R2 C-tail. The expression of R1a$^{BBS-ASA}$R2ΔCT in GIRK cells revealed co-localization of subunits on the cell surface by immunostaining for the Myc tag on R1a and the FLAG tag on R2 (data not shown). At room temperature, R1a$^{BBS-ASA}$R2ΔCT constitutively internalized at a rate (Fig. 6, *A*–*C*) and extent (Fig. 6, *A*, *B*, and *D*) that were indistinguishable from R1a$^{BBS-ASA}$ (Table 1). The rate was significantly faster than that for R1aR2^{BBS} and R2^{BBS} (Fig. 6*C*), and the extent of internalization was significantly greater compared with R1a^{BBS}R2, R1aR2^{BBS}, R2^{BBS}, and R1a$^{BBS-ASA,L889A,L890A}$.

Therefore, these results strongly suggest that R2 subunits determine the rate of constitutive internalization of the heterodimer by masking a dominant dileucine motif internalization signal on the R1a coiled-coil domain. This is most likely to occur by interaction between the C-tails of R1a and R2.

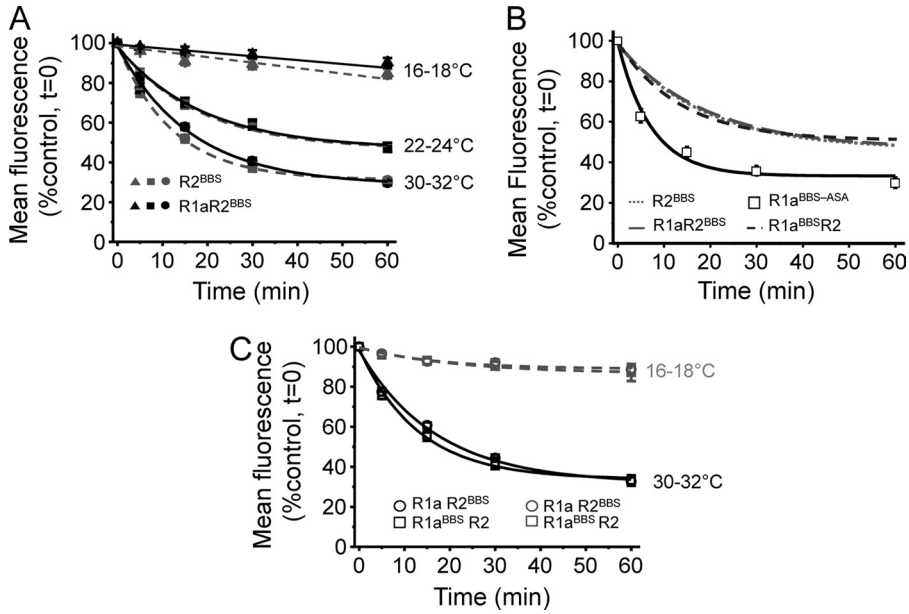

FIGURE 5. **R2 subunits slow the rate of GABA$_B$ receptor internalization.** *A*, rate and extent of internalization for BTX-AF555-tagged R2^{BBS} (*gray*) or R1aR2^{BBS} (*black*) at 16–18 °C (▲), 22–24 °C (■), and 30–32 °C (●) (n = 5–13). GIRK cells expressing R2^{BBS} or R1aR2^{BBS} were incubated in 3 μg/ml BTX-AF555 for 10 min at room temperature prior to imaging over 0–60 min. *B*, comparison of internalization of R1a$^{BBS-ASA}$ with R1a^{BBS}R2, R1aR2^{BBS}, and R2^{BBS} (data taken from *A* and Fig. 1*A*) at 22–24 °C. *C*, rate of internalization of BTX-AF555-tagged R1a^{BBS}R2 (□) and R1aR2^{BBS} (○) receptors at 16–18 °C and 30–32 °C in live hippocampal neurons (n = 6 - 14). Neurons (14–21 DIV) expressing R1aR2^{BBS} and eGFP were incubated in 1 mM D-tubocurarine for 5 min followed by 3 μg/ml BTX-AF555 for 10 min at room temperature before imaging at 16–18 or 30–32 °C.

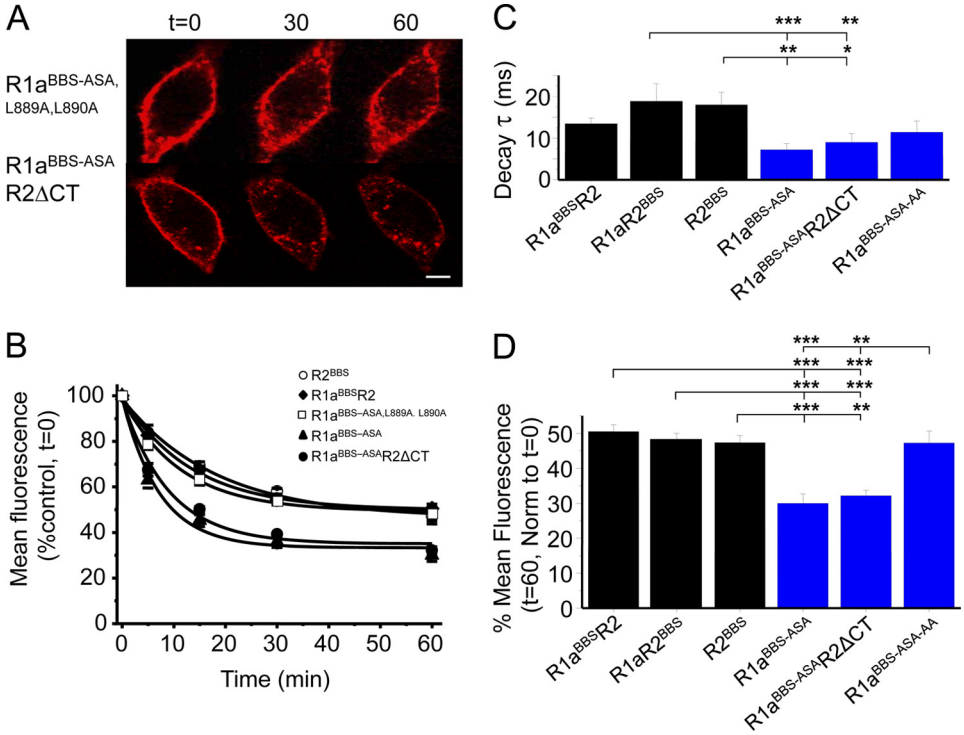

FIGURE 6. **Dileucine motif on R1a determines the rate of internalization.** *A*, GIRK cells expressing R1a$^{BBS-ASA,L889A,L890A}$ (*top*) or R1a$^{BBS-ASA}$R2ΔCT (*bottom*) were incubated in 3 μg/ml BTX-AF555 for 10 min at room temperature and imaged over 0–60 min at room temperature. *Scale bar*, 5 μm. *B*, rates of constitutive internalization for R2^{BBS}, R1a^{BBS}R2, R1a$^{BBS-ASA,L889A,L890A}$, R1a$^{BBS-ASA}$, and R1a$^{BBS-ASA}$R2ΔCT receptors (n = 6). *C*, decay time constants for the surface membrane fluorescence for the subunits indicated, where R1a$^{BBS-ASA-L889A,L890A}$ = R1a$^{BBS-ASA-AA}$. *D*, extent of internalization for the subunits indicated. *, $p < 0.05$; **, $p < 0.01$; ***, $p < 0.001$, one-way analysis of variance. *Error bars*, S.E.

Dual Labeling of R1a and R2 with Different BTX-linked Fluorophores—The rates and extents of internalization for GABA$_B$ receptor heterodimers, monitored with a BBS tag on either R1a (R1a^{BBS}R2) or R2 (R1aR2^{BBS}), are very similar, suggesting that most are internalized as heterodimers. To unequivocally demonstrate this required the simultaneous labeling of R1a and R2 with BTX linked to different fluorophores. However, for dual labeling, the BBS on one of the subunits must be chemically protected while the BBS on the other subunit remains accessible. To enable this, we substituted two vicinal

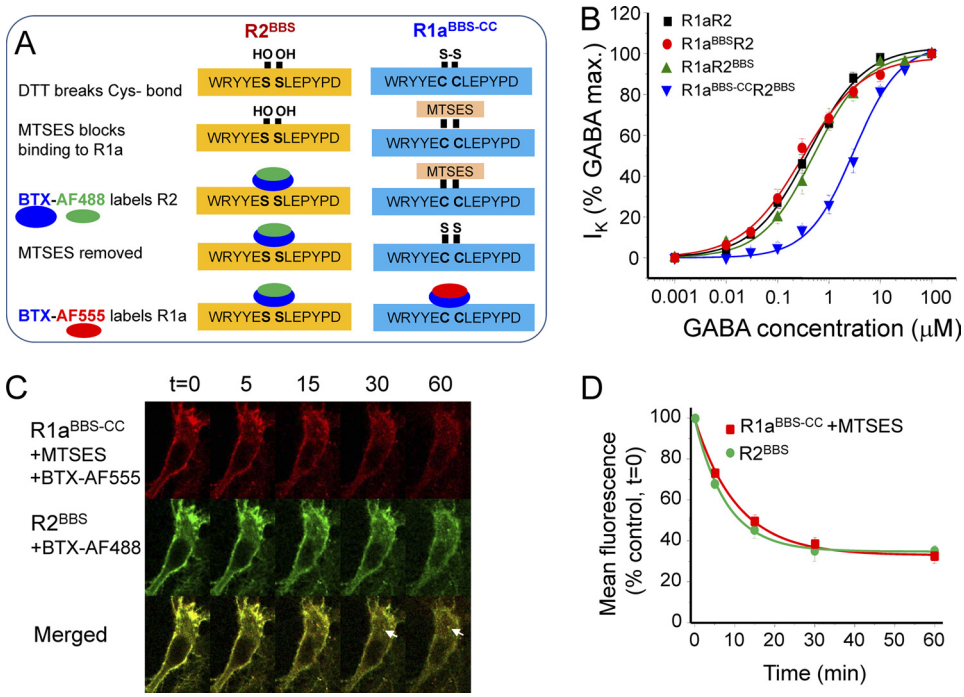

FIGURE 7. **GABA$_B$ receptors are constitutively internalized as heterodimers.** *A*, schematic for the dual labeling strategy for R2 (wild-type BBS, *left*) and R1a (mutant BBS, *right*) subunits. *B*, GABA concentration response curves for R1aR2, R1aR2^{BBS}, R1a^{BBS}R2, and R1a^{BBS-CC}R2^{BBS} expressed in GIRK cells (n = 7–13). *C*, hippocampal neurons (14–21 DIV) expressing R1a^{BBS-CC}R2^{BBS} were incubated in 1 mM D-tubocurarine for 5 min followed by 200 μM DTT for 30 min at room temperature, 20 μM MTSES for 5 min, 3 μg/ml BTX-AF488 for 10 min at 4 °C, 5 mM DTT for 5 min at room temperature, and 3 μg/ml BTX-AF555 for 10 min at 4 °C and imaged at different times at 30–32 °C. The *arrowheads* indicate some examples of co-localized and internalized R1a and R2 subunits. *D*, rate of constitutive internalization of BTX-AF488-tagged R2^{BBS} and BTX-AF555-tagged R1a^{BBS-CC} receptors (n = 5).

serines in the BBS of R1a^{BBS} for cysteines (R1a^{BBS-CC}; Fig. 7*A*). By covalent labeling of the Cys residues using a sulfhydryl reagent, the binding of BTX to R1a was prevented, whereas binding to the wild-type BBS on R2 could proceed unhindered. BTX binding to R1a was subsequently restored by removing the protective sulfhydryl reagent using DTT (Fig. 7*A*).

The structural integrity of the modified BBS was confirmed by BTX-AF555 labeling of R1a^{BBS-CC}R2 in GIRK cells. The binding was selective, and the fluorescence intensity was slightly reduced compared with labeled R1a^{BBS}R2 (data not shown). Reducing the Cys bridge with DTT did not improve the fluorescence intensity for R1a^{BBS-CC}R2. To prevent BTX-AF555 binding to R1a^{BBS-CC}, the two vicinal Cys residues were reduced (breaking a Cys-Cys bridge) using 200 μM DTT for 30 min at room temperature before the application of 20 μM MTSES for 5 min at 4 °C. Under these conditions, the surface labeling by BTX-AF555 was minimal (supplemental Fig. 6).

Having established that binding to R1a^{BBS-CC} was prevented by MTSES, the protecting group was removed with 5 mM DTT for 5 min at room temperature. Subsequent incubation with BTX-AF555 for 10 min at room temperature significantly recovered surface fluorescence, indicating that BTX-AF555 was binding to R1a^{BBS-CC} (supplemental Fig. 6).

Whole-cell recording was used to determine the impact of the Cys residues in the BBS on the function of R1a^{BBS-CC}R2^{BBS}. Following serine substitution, there is a small reduction in GABA potency for activating inwardly rectifying potassium currents with an 8-fold shift in the EC$_{50}$ to 3.2 ± 0.37 μM (n = 6; Fig. 7*B*). This was not sufficiently different from that for R1a^{BBS} to affect its use as a tag for monitoring the movement of GABA$_B$ receptors.

We then used dual BTX labeling with R1a^{BBS-CC}R2^{BBS} to study whether the two GABA$_B$ receptor subunits were internalized as heterodimers. Following the protection of R1a^{BBS-CC} with MTSES, BTX-AF488 was applied for 10 min at 4 °C to label surface R2^{BBS}. After deprotection of R1a^{BBS-CC}, BTX-AF555 was applied for 10 min at 4 °C to label surface R1a^{BBS-CC} (Fig. 7*A*).

The cells were incubated at 30–32 °C, and BTX-AF488 and BTX-AF555 labeling in live cells was detected at different time points. Notably, R1a and R2 were co-localized to intracellular compartments at 15–60 min (Fig. 7*C*). No intracellular compartments were decorated with only one or the other of the fluorophores. The rates and extents of internalization for the labeled R1a and R2 subunits (Fig. *7D* and Table 1) were also similar. Taken together, these data strongly suggest that the majority of R1a and R2 subunits are mostly internalized as heterodimers.

DISCUSSION

Slow synaptic inhibition in the CNS relies on the hetero-oligomerization of R1 and R2 GABA$_B$ receptor subunits. This links the transmitter binding site of R1 with the G-protein signaling properties possessed by R2. Although it is well established that heterodimerization enables the trafficking of R1 subunits to the cell surface, what controls GABA$_B$ receptor surface stability thereafter is less well understood. The ability to track the real-time movement of R1 and R2 subunits in live cells

using the BBS and the fluorophore-conjugated α-BTX provides opportunities for investigating the role of R2 in the molecular mechanisms underlying cell surface receptor stability. Inserting the BBS does not affect the trafficking properties of the $GABA_B$ receptors *per se* by comparison with other studies monitoring internalization using biotinylation (12) of antibody labeling (14).

R2 Is a Regulator of $GABA_B$ Receptor Internalization—The fast rate of internalization of $R1a^{BBS\text{-}ASA}$ homomers became evident once the ER retention motif had been substituted, allowing R1a access to the surface membrane. The moderating influence of R2 was apparent by extending the use of the BBS tagging strategy to insert a functionally silent, high affinity BBS into the N-terminal domain of R2 subunits. Tracking the real-time movement of R2 subunits, for the first time independently from R1a, revealed that its internalization rate was notably slow. Indeed, the rates of internalization for $R1a^{BBS}R2$, $R1aR2^{BBS}$, and $R2^{BBS}$ were comparable with and significantly slower than for $R1a^{BBS\text{-}ASA}$. Independent of which subunit was tagged with the BBS, the R2 subunit slowed the rate and reduced the extent of internalization. Thus, heterodimerization will provide greater stability for cell surface $GABA_B$ receptors, thereby enhancing inhibition. The equivalent rates of internalization noted when R2 was present in the $GABA_B$ receptor imply that R1aR2 heterodimers do not internalize as a weighted mean of the rates for R1a and R2 but are determined by the internalization rate of R2 alone.

The rates of internalization, measured by fluorophore-conjugated BTX labeling, are likely to accurately reflect $GABA_B$ receptor trafficking for three reasons. First, BTX binds with relatively high affinity to the BBS inserted in either the R1a or R2 subunits. The apparent affinity compares well (11-fold lower) with that measured for the native α-BTX binding site on the nicotinic acetylcholine $\alpha7/5HT_{3A}$ chimera. Thus, significant dissociation of the fluorophore from the $GABA_B$ receptor is unlikely. Second, there is very little constitutive internalization of $GABA_B$ receptor monomers and heterodimers at low temperatures, which are non-permissive conditions for internalization. This changes at room temperature and PT, where heterodimers and homomers internalized rapidly in a temperature-dependent manner. Third, the reduction in cell surface fluorescence is not a consequence of photobleaching of BTX-AF555 because this is negligible (<10%) with the scanning protocols used to follow receptor mobility.

Structural Motif Promoting Rapid $GABA_B$ Receptor Internalization—The rapid internalization of $R1a^{BBS\text{-}ASA}$ compared with $R2^{BBS}$ was likely to be caused by one or more intracellular motifs specifically located on the R1a subunit. The C-tail was designated as the prime location for controlling receptor internalization because of its length and its engagement with the equivalent tail in the R2 subunit, which also influences the rate of internalization of the heterodimer.

By truncating the C-tail of $R1a^{BBS\text{-}ASA}$ after the seventh transmembrane domain, the rate of internalization was reduced toward that of $R1^{BBS}R2$, identifying the domain location of an endocytic motif that increased the rate of constitutive internalization of $R1a^{BBS\text{-}ASA}$ compared with R1aR2. By replacing the dileucine motif (Leu^{889}, Leu^{890}) in $R1a^{BBS\text{-}ASA,L889A,L890A}$, the rate and extent of constitutive internalization became comparable with that for $R2^{BBS}$ and R1aR2. By contrast, co-assembly of $R1a^{BBS}$ with R2ΔCT produced receptors exhibiting similar rates and extents of internalization to $R1a^{BBS\text{-}ASA}$, discounting the possibility that the ASA motif was serving as an endocytic signal.

For the R1aR2 heterodimer, the dileucine motif did not increase the rate of internalization. This may be a consequence of the R2 subunit C-tail. Its truncation in R2ΔCT and co-expression with $R1a^{BBS\text{-}ASA}$ no longer slowed the rate and extent of internalization to that of the R2 homomer but proceeded at the same rate and to the same extent as that of $R1a^{BBS\text{-}ASA}$ homomers. The most plausible explanation is that the R2 subunit determines the rate and extent of internalization of heterodimers by masking the dileucine motif upon coassembly with residues from its C-tail. The dileucine motif is suitably positioned in the coiled-coil domain, a major site of interaction between R1 and R2 (32, 33).

The importance of the dileucine motif on R1a trafficking is exemplified by its previous description as an interaction motif for Msec7-1 (30), which is a guanine nucleotide exchange factor of the ADP-ribosylation factor proteins. These proteins are known to play an important role in vesicular trafficking in all eukaryotic cells (34). Indeed, the overexpression of Msec7-1 up-regulates the levels of $R1^{ASA}$ on the cell surface of COS-7 cells via an interaction with the dileucine motif. It is conceivable that Msec7-1 could serve as an adapter for $GABA_B$ receptor internalization by interacting with the dileucine motif, causing $R1a^{ASA}$ receptors to be internalized faster and to a greater extent than R1aR2. An isoleucine-leucine pair is also present on the R2 subunit (Ile^{853}, Leu^{854}), but this motif appears to play no role in $GABA_B$ receptor trafficking despite the R2 subunit C-tail influencing the targeting of assembled receptors to specific neuronal compartments (35).

Cycling of $GABA_B$ Receptors—The rate and extent of internalization were notably increased for R1a homomers when the RSR retention motif was removed. Co-expression with R2 nullified this effect unless the C-tail for R2 was truncated. By combining the rates of receptor movement measured in this study with others, it is possible to construct a kinetic model for the trafficking of $GABA_B$ receptors (Fig. 8*A*). The main elements of the model include rates for $GABA_B$ receptor endocytosis from the surface membrane (k_{endo}; this study), synthesis and insertion of new receptors from the Golgi stack/ER (k_{in}; taken from Ref. 13), degradation of endocytosed receptors (k_{degrad}), recycling of receptors back to the surface membrane (k_{recyc}), and photobleaching of the BTX attached fluorophore (k_{pb}; this study (Fig. 8*A*)). The removal of $GABA_B$ receptors from the surface membrane (as measured by the loss of surface fluorescence) was a function of the rate of insertion ($\tau = 7.8$ min (13)) and the rate of endocytosis ($\tau = 15$ min for R1aR2 heteromers), with photobleaching ($\tau = 98$ min) having a negligible contribution. To ensure that a plateau phase develops requires that a proportion of receptors must recycle back to the cell surface. This rate was empirically determined to reproduce the experimental data, being set to $\tau = 25$ min with up to 40% of internalized receptors being returned to the surface. A proportion are considered to be degraded from the internalized pool, and this

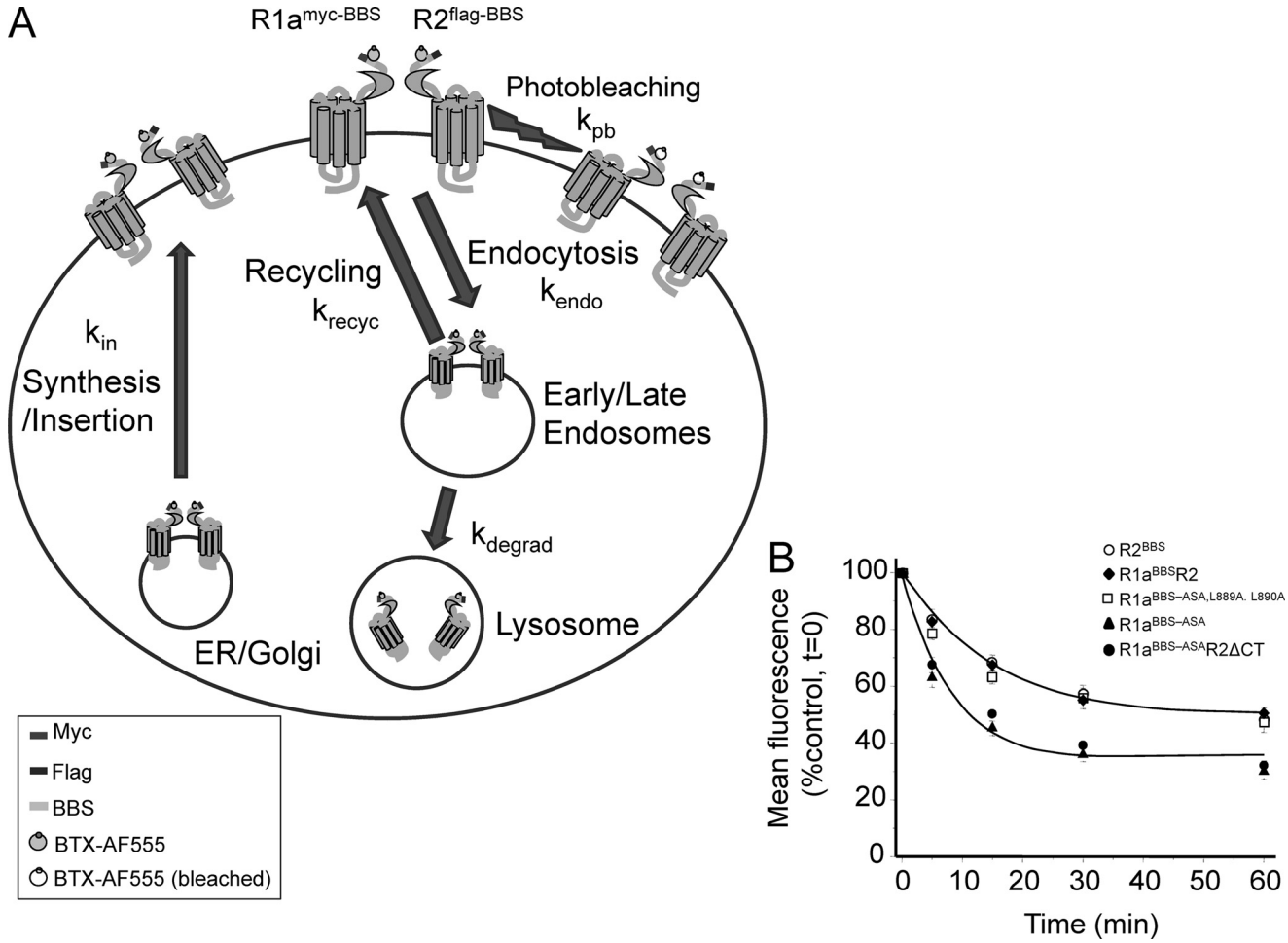

FIGURE 8. **Trafficking model for GABA$_B$ receptors.** *A*, schematic diagram that illustrates the trafficking of GABA$_B$ receptors from the cell surface to early/late endosomes and onto lysosomes. The surface replenishment pathway involves the recycling of receptors and the synthetic pathway from the Golgi stack. The respective rate constants and key for the GABA$_B$ receptors are indicated. *B*, rates of constitutive internalization for R2^{BBS}, R1a^{BBS}R2, R1a$^{BBS-ASA,L889A,L890A}$, R1a$^{BBS-ASA}$, and R1a$^{BBS-ASA}$R2ΔCT receptors, taken from Fig. 6*B*. The curve fits are generated using the model in *A* with $k_{endo} = 0.067$ min^{-1}, $k_{in} = 0.128$ min^{-1}, $k_{pb} = 0.01$ min^{-1}, $k_{recyc} = 0.04$ min^{-1}, $k_{degrad} = 0.0083$ min^{-1} (for R1aR2; *blue*) with 45% of receptors recycling, and $k_{endo} = 0.11$ min^{-1}, $k_{in} = 0.128$ min^{-1}, $k_{pb} = 0.01$ min^{-1}, $k_{recyc} = 0.04$ min^{-1}, $k_{degrad} = 0.0083$ min^{-1} (for R1a$^{BBS-ASA}$; *red*) with 30% of receptors recycling.

was set empirically at 20% with a $\tau = 120$ min. Given these boundary conditions, and apart from changing the rate of endocytosis, the plateau steady-state phases of the decay curves involving R1a$^{BBS-ASA}$ and R1a$^{BBS-ASA}$R2δCT, compared with R1aR2 and R2^{BBS} (Fig. 6*B*), are most easily accounted for by changes in receptor recycling (Fig. 8*B*). Although increased receptor insertion will also affect the steady state, when the rates are increased, this slows the rate of internalization, often causing an inflection on the decay phase that is not observed experimentally. Changes to the rate of degradation can also affect the steady-state, but under the conditions of the model, large excursions in the extent of degradation have minimal effect on the steady state. Overall, receptor recycling appears the likeliest cause for moderating the extent of receptor endocytosis.

Mulitple Roles for GABA$_B$ Receptor Heterodimerization—The GABA$_B$ receptor was the first example of a GPCR that required heterodimerization to support ligand binding and G-protein coupling (32, 36). Although the precise subunit stoichiometry (or stoichiometries) for GABA$_B$ receptors has not been resolved, primary heterodimerization between R1 and R2 performs at least three distinct roles. First, to link ligand binding to downstream signaling, the ligand binding site located in the VFTM of R1 needs to be co-assembled with the G-protein coupling domain located in the intracellular loops of R2 (37–40). Second, an interaction between the VFTMs of R1 and R2 is important to create a high affinity GABA binding site (41), and any disruption to this extracellular interaction abolishes subsequent G-protein coupling (42). Third, R1 requires R2 to act as a chaperone to reach the cell surface (9) because of the ER retention motif in R1 (8). Here, we add another important role for heterodimerization in which R2 determines the rate and extent of internalization of heterodimers by masking the dileucine motif in the C-tail coiled-coil domain of R1a.

As predicted from studies using fixed tissue (12, 14), the process of constitutive endocytosis in live cells, monitored with the tagged BBS, proceeded via clathrin- and dynamin-dependent mechanisms, which were inhibited by either chloropromazine or dynasore. The importance of the dileucine motif for GABA$_B$ receptor trafficking is highlighted by its trafficking role in other proteins and interactions with adapter proteins for clathrin-mediated endocytosis (43).

The coupling between R1a and R2 is sufficiently tight such that both subunits are internalized together, dispensing with the need to dissociate beforehand in the plane of the cell surface (31). This aspect was unequivocally demonstrated by extending the versatility of the BBS tagging method to enable dual labeling of the R1a and R2 subunits with BTX conjugated to discrete fluorophores.

Thus, in conclusion, the new role for R2 subunits in determining the rate of internalization of R1aR2 denotes R2 as a major determinant of cell surface $GABA_B$ receptor stability. This will influence the efficacy of slow synaptic inhibition in the CNS by slowing the removal of receptors from the cell surface. This is a desirable property for G-protein-coupled receptors that are generally considered to perform a housekeeping role in providing background, low efficacy inhibition following GABA spillover from inhibitory synapses.

Acknowledgment—We thank Stuart Lansdell for help with the radioligand binding experiments.

REFERENCES

1. Enna, S. J., and Bowery, N. G. (2004) *Biochem. Pharmacol* **68,** 1541–1548
2. Bowery, N. G. (1989) *Trends Pharmacol. Sci.* **10,** 401–407
3. Bettler, B., Kaupmann, K., Mosbacher, J., and Gassmann, M. (2004) *Physiol. Rev.* **84,** 835–867
4. Bowery, N. G., and Enna, S. J. (2000) *J. Pharmacol. Exp. Ther.* **292,** 2–7
5. Marshall, F. H., Jones, K. A., Kaupmann, K., and Bettler, B. (1999) *Trends Pharmacol. Sci.* **20,** 396–399
6. Villemure, J. F., Adam, L., Bevan, N. J., Gearing, K., Chénier, S., and Bouvier, M. (2005) *Biochem. J.* **388,** 47–55
7. Maurel, D., Comps-Agrar, L., Brock, C., Rives, M. L., Bourrier, E., Ayoub, M. A., Bazin, H., Tinel, N., Durroux, T., Prézeau, L., Trinquet, E., and Pin, J. P. (2008) *Nat. Methods* **5,** 561–567
8. Margeta-Mitrovic, M., Jan, Y. N., and Jan, L. Y. (2000) *Neuron* **27,** 97–106
9. Couve, A., Filippov, A. K., Connolly, C. N., Bettler, B., Brown, D. A., and Moss, S. J. (1998) *J. Biol. Chem.* **273,** 26361–26367
10. Fairfax, B. P., Pitcher, J. A., Scott, M. G., Calver, A. R., Pangalos, M. N., Moss, S. J., and Couve, A. (2004) *J. Biol. Chem.* **279,** 12565–12573
11. Perroy, J., Adam, L., Qanbar, R., Chénier, S., and Bouvier, M. (2003) *EMBO J.* **22,** 3816–3824
12. Vargas, K. J., Terunuma, M., Tello, J. A., Pangalos, M. N., Moss, S. J., and Couve, A. (2008) *J. Biol. Chem.* **283,** 24641–24648
13. Wilkins, M. E., Li, X., and Smart, T. G. (2008) *J. Biol. Chem.* **283,** 34745–34752
14. Grampp, T., Sauter, K., Markovic, B., and Benke, D. (2007) *J. Biol. Chem.* **282,** 24157–24165
15. Grampp, T., Notz, V., Broll, I., Fischer, N., and Benke, D. (2008) *Mol. Cell Neurosci.* **39,** 628–637
16. Arancibia-Cárcamo, I. L., Yuen, E. Y., Muir, J., Lumb, M. J., Michels, G., Saliba, R. S., Smart, T. G., Yan, Z., Kittler, J. T., and Moss, S. J. (2009) *Proc. Natl. Acad. Sci. U.S.A.* **106,** 17552–17557
17. Harel, M., Kasher, R., Nicolas, A., Guss, J. M., Balass, M., Fridkin, M., Smit, A. B., Brejc, K., Sixma, T. K., Katchalski-Katzir, E., Sussman, J. L., and Fuchs, S. (2001) *Neuron* **32,** 265–275
18. Donnelly, S. R., Hawkins, T. E., and Moss, S. E. (1999) *Hum. Mol. Genet.* **8,** 1723–1728
19. Xia, Z., Dudek, H., Miranti, C. K., and Greenberg, M. E. (1996) *J. Neurosci.* **16,** 5425–5436
20. Connolly, C. N., Kittler, J. T., Thomas, P., Uren, J. M., Brandon, N. J., Smart, T. G., and Moss, S. J. (1999) *J. Biol. Chem.* **274,** 36565–36572
21. Macia, E., Ehrlich, M., Massol, R., Boucrot, E., Brunner, C., and Kirchhausen, T. (2006) *Dev. Cell* **10,** 839–850
22. de Hoop, M. J., Huber, L. A., Stenmark, H., Williamson, E., Zerial, M., Parton, R. G., and Dotti, C. G. (1994) *Neuron* **13,** 11–22
23. Mohrmann, K., and van der Sluijs, P. (1999) *Mol. Membr. Biol.* **16,** 81–87
24. Zerial, M., and McBride, H. (2001) *Nat. Rev. Mol. Cell. Biol.* **2,** 107–117
25. Stenmark, H., and Olkkonen, V. M. (2001) *Genome Biol.* **2,** REVIEWS3007
26. Méresse, S., Gorvel, J. P., and Chavrier, P. (1995) *J. Cell Sci.* **108,** 3349–3358
27. Kantamneni, S., Holman, D., Wilkinson, K. A., Corrêa, S. A., Feligioni, M., Ogden, S., Fraser, W., Nishimune, A., and Henley, J. M. (2008) *J. Neurochem.* **107,** 86–95
28. Terunuma, M., Vargas, K. J., Wilkins, M. E., Ramírez, O. A., Jaureguiberry-Bravo, M., Pangalos, M. N., Smart, T. G., Moss, S. J., and Couve, A. (2010) *Proc. Natl. Acad. Sci. U.S.A.* **107,** 13918–13923
29. Eiselé, J. L., Bertrand, S., Galzi, J. L., Devillers-Thiéry, A., Changeux, J. P., and Bertrand, D. (1993) *Nature* **366,** 479–483
30. Restituito, S., Couve, A., Bawagan, H., Jourdain, S., Pangalos, M. N., Calver, A. R., Freeman, K. B., and Moss, S. J. (2005) *Mol. Cell Neurosci.* **28,** 747–756
31. Kammerer, R. A., Frank, S., Schulthess, T., Landwehr, R., Lustig, A., and Engel, J. (1999) *Biochemistry* **38,** 13263–13269
32. White, J. H., Wise, A., Main, M. J., Green, A., Fraser, N. J., Disney, G. H., Barnes, A. A., Emson, P., Foord, S. M., and Marshall, F. H. (1998) *Nature* **396,** 679–682
33. Kuner, R., Köhr, G., Grünewald, S., Eisenhardt, G., Bach, A., and Kornau, H. C. (1999) *Science* **283,** 74–77
34. Jackson, T. R., Kearns, B. G., and Theibert, A. B. (2000) *Trends Biochem. Sci.* **25,** 489–495
35. Pooler, A. M., Gray, A. G., and McIlhinney, R. A. (2009) *Eur. J. Neurosci.* **29,** 869–878
36. Kaupmann, K., Malitschek, B., Schuler, V., Heid, J., Froestl, W., Beck, P., Mosbacher, J., Bischoff, S., Kulik, A., Shigemoto, R., Karschin, A., and Bettler, B. (1998) *Nature* **396,** 683–687
37. Margeta-Mitrovic, M., Jan, Y. N., and Jan, L. Y. (2001) *Proc. Natl. Acad. Sci. U.S.A.* **98,** 14649–14654
38. Duthey, B., Caudron, S., Perroy, J., Bettler, B., Fagni, L., Pin, J. P., and Prézeau, L. (2002) *J. Biol. Chem.* **277,** 3236–3241
39. Havlickova, M., Prezeau, L., Duthey, B., Bettler, B., Pin, J. P., and Blahos, J. (2002) *Mol. Pharmacol.* **62,** 343–350
40. Robbins, M. J., Calver, A. R., Filippov, A. K., Hirst, W. D., Russell, R. B., Wood, M. D., Nasir, S., Couve, A., Brown, D. A., Moss, S. J., and Pangalos, M. N. (2001) *J. Neurosci.* **21,** 8043–8052
41. Galvez, T., Duthey, B., Kniazeff, J., Blahos, J., Rovelli, G., Bettler, B., Prézeau, L., and Pin, J. P. (2001) *EMBO J.* **20,** 2152–2159
42. Rondard, P., Huang, S., Monnier, C., Tu, H., Blanchard, B., Oueslati, N., Malhaire, F., Li, Y., Trinquet, E., Labesse, G., Pin, J. P., and Liu, J. (2008) *EMBO J.* **27,** 1321–1332
43. Wolfe, B. L., and Trejo, J. (2007) *Traffic* **8,** 462–470